



THE COMBINED EFFECT OF PRECESSION AND CONVECTION ON THE DYNAMO ACTION

XING WEI

Institute of Natural Sciences and Department of Physics and Astronomy, Shanghai Jiao Tong University, Shanghai 200240, China; xing.wei@sjtu.edu.cn
Princeton University Observatory, Princeton, NJ 08544, USA

Received 2016 January 9; revised 2016 May 8; accepted 2016 June 9; published 2016 August 15

ABSTRACT

To understand the generation of the Earth’s magnetic field and those of other planets, we numerically investigate the combined effect of precession and convection on dynamo action in a spherical shell. Convection alone, precession alone, and the combined effect of convection and precession are studied at the low Ekman number at which the precessing flow is already unstable. The key result is that although precession or convection alone are not strong enough to support the dynamo action, the combined effect of precession and convection can support the dynamo action because of the resonance of precessional and convective instabilities. This result may explain why the geodynamo has been maintained for such a long time compared to the Martian dynamo.

Key words: convection – dynamo

1. INTRODUCTION

The magnetic fields of astronomical bodies are generated through the dynamo action, namely, the motion of electrically conducting fluid shears and twists magnetic field lines to create new field lines to offset magnetic diffusion. For the dynamo in the Earth’s core, i.e., the geodynamo, thermal and compositional convection is believed to be the major power, where the differential rotation and helical motion combine to induce the dynamo action. The convection dynamo has been extensively studied since the 1970s, e.g., by Busse (1978), Hollerbach (1996), Zhang & Schubert (2000), Roberts & Glatzmaier (2000), Jones (2011), etc. On the other hand, Bullard & Gellman (1954) discussed the possibility of a precession driven geodynamo, and Malkus (1968) pointed out that the flow instabilities driven by precession could power the geodynamo. The most recent work shows that convection in the Earth’s core may not be sufficiently strong for heat transfer as anticipated in earlier studies (Olson 2013), which implies that the Earth’s precession might be the major power for the geodynamo. Moreover, magnetic records show that geomagnetic dipole reversals are statistically correlated to the Earth’s orbital eccentricity (Yamazaki & Oda 2002), which implies that the Earth’s precession also plays an important role in the dipole reversals. These geophysical applications motivate the study of the precession dynamo.

The precessing flow in spheroidal geometry was studied by Poincaré (1910) for inviscid fluid and by Busse (1968) for viscous fluid. Recently, the study of precessing flow has attracted much attention, e.g., the asymptotic study by Zhang et al. (2014), the numerical studies by Cébron et al. (2010) and Hollerbach et al. (2013), and the experimental studies by Noir et al. (2003), Lavorel & Le Bars (2010), Goto et al. (2014), Lin et al. (2014), etc. However, not many studies have been carried out for the precession dynamo because of the complex flow structure, e.g., the inertial waves spawned from the critical latitude, the thin internal shear layers, the triad resonance of instabilities, etc. (Kerswell 1993; Tilgner 2007).

Tilgner (2005) carried out the first numerical calculation on the precession dynamo in spherical geometry using the spectral method. It was found that both the laminar precessing flow at high Ekman number and the unstable precessing flow at low Ekman number can induce the dynamo. In the former, the

dynamo is powered by the poloidal flow arising from the Ekman layer, and in the latter it is powered by the instabilities of the precessing flow. Later, Wu & Roberts (2009) carried out finite difference calculations in spheroidal geometry, and Ernst-Hullermann et al. (2013, pp. 208–243) carried out finite volume calculations in ellipsoidal geometry.

A question then arose. What would be the combined effect of precession and convection on the dynamo action? Wei & Tilgner (2013) carried out numerical calculations on the hydrodynamic interaction of precession and convection in a spherical shell. It was found that the two driving mechanisms for the dynamo can destabilize each other, namely, their mutual interaction leads to a more unstable flow because of the resonance of the two instabilities (see the details in Wei & Tilgner 2013). Usually, the flow instabilities favor dynamo action, and thus it seems plausible that the combined effect of precession and convection may facilitate the onset of the dynamo and lead to more efficient dynamo action.

In this paper, we extend the numerical calculations of the precession dynamo in Tilgner (2005) and of the precession-convection flow in Wei & Tilgner (2013) to the precession-convection dynamo. We use the same numerical setup and code as in these two previous papers, i.e., the same linear stratification profile and the same precession angle of 60° . In Section 2, the mathematical equations are formulated and the numerical method is introduced. In Section 3, the numerical results are shown and discussed. In Section 4, we provide a summary and briefly discuss possible applications to geomagnetism, the Martian magnetic field, magnetic fields in small bodies, and further opportunities for study.

2. EQUATIONS

Our numerical setup is identical to that in Tilgner (2005) and Wei & Tilgner (2013). Suppose that we have a conducting fluid in a spherical shell with aspect ratio r_i/r_o . The spherical shell spins at a rate Ω_s about its symmetric axis (the z axis) and precesses at a rate Ω_p about an inclined axis with angle β to the z axis. In the frame attached to the boundary, the unit vector of the precession axis is expressed in the Cartesian coordinate system (x, y, z) as

$$\hat{\Omega}_p = \sin \beta \cos t \hat{x} - \sin \beta \sin t \hat{y} + \cos \beta \hat{z}, \quad (1)$$

where the hat denotes the unit vector. Meanwhile, we impose a background temperature T_b and assume that it has a linear profile

$$T_b = \frac{T_o - T_i}{d}(r - r_o) + T_o, \quad (2)$$

where T_o and T_i are the temperature, respectively, at r_o and r_i , and d is the thickness of the spherical shell. The temperature gradient $(T_o - T_i)/d$ is negative (i.e., unstable stratification) for convection. This linear temperature profile is maintained by a heat source inversely proportional to the radius. In addition to the linear profile, we can assume other profiles maintained by different heat sources. We choose the linear profile because it is simple in terms of numerics, namely, in the physical space the grids near the boundaries are not required to be dense, such that the Chebyshev collocation points we use in the radial direction are sufficiently dense to resolve the linear profile.

We make use of the Boussinesq approximation that the density variation is only considered in the buoyancy force and is proportional to the temperature deviation $\Theta = T - T_b$. Then, the dimensionless Navier–Stokes equation in the frame attached to the boundary reads

$$\begin{aligned} \frac{\partial \mathbf{u}}{\partial t} + \mathbf{u} \cdot \nabla \mathbf{u} = & -\nabla \Phi + Ek \nabla^2 \mathbf{u} + 2\mathbf{u} \times (\hat{\mathbf{z}} + Po \hat{\Omega}_p) \\ & + Po(\hat{\mathbf{z}} \times \hat{\Omega}_p) \\ & \times \mathbf{r} + \widetilde{Ra} \Theta \mathbf{r} + (\nabla \times \mathbf{B}) \times \mathbf{B}, \end{aligned} \quad (3)$$

where all of the curl-free terms are absorbed into the total potential Φ . On the right-hand side of Equation (3), the second term is the viscous force, the third term is the Coriolis force due to global rotation, the fourth term is the Poincaré force due to precession and it drives the precessing flow, the fifth term is the buoyancy force due to stratification, and the last term is the Lorentz force due to the magnetic field. The dimensionless temperature deviation equation reads

$$\frac{\partial \Theta}{\partial t} + \mathbf{u} \cdot \nabla \Theta = \frac{Ek}{Pr} \nabla^2 \Theta + u_r. \quad (4)$$

On the right-hand side of Equation (4), the inhomogeneous term u_r derived from the advection term $\mathbf{u} \cdot \nabla T_b$ causes the temperature deviation. The dimensionless magnetic induction equation reads

$$\frac{\partial \mathbf{B}}{\partial t} = \nabla \times (\mathbf{u} \times \mathbf{B}) + \frac{Ek}{Pm} \nabla^2 \mathbf{B}. \quad (5)$$

In the above dimensionless Equations (3)–(5), the normalization is as follows. Length is normalized with the shell thickness d , time with the inverse of the rotation rate Ω_s^{-1} , velocity with $\Omega_s d$, temperature deviation with $T_i - T_o$, and the magnetic field with $\sqrt{\rho \mu} \Omega_s d$ (where ρ is the fluid density and μ the magnetic permeability). There are five dimensionless parameters governing the system. The Ekman number $Ek = \nu / (\Omega_s d^2)$ measures the ratio of the viscous timescale to the spin timescale, the Poincaré number $Po = \Omega_p / \Omega_s$ measures the ratio of the precession rate to the spin rate, the rotational Rayleigh number $\widetilde{Ra} = \alpha g_o (T_i - T_o) / (\Omega_s^2 r_o)$ (where α is the thermal expansion coefficient and g_o the gravitational acceleration at r_o) measures the square of the ratio of the buoyancy frequency to the spin rate, the Prandtl number $Pr = \nu / \kappa$

measures the ratio of the viscosity to the thermal diffusivity, and the magnetic Prandtl $Pm = \nu / \eta$ measures the ratio of the viscosity to the magnetic diffusivity. It should be noted that what we use to measure the strength of the convection is the rotational Rayleigh number, not the conventional Rayleigh number $Ra = \alpha g_o (T_i - T_o) r_o^3 / \nu \kappa$. They are related through

$$\begin{aligned} Ra &= \frac{\alpha g_o (T_i - T_o) d^3}{\nu \kappa} = \frac{\alpha g_o (T_i - T_o)}{\Omega_s^2 r_o} \frac{\Omega_s^2 d^4}{\nu^2} \frac{\nu}{\kappa} \frac{r_o}{d} \\ &= \widetilde{Ra} Ek^{-2} Pr \frac{r_o}{d}. \end{aligned} \quad (6)$$

The aspect ratio is given as 0.1 to minimize the effect of the inner core, and the precession angle β is given as 60° , as in Tilgner (2005) and Wei & Tilgner (2013), such that precession has a noticeable effect.

The velocity boundary condition is no-slip $\mathbf{u} = 0$ at the outer boundary (precession in spherical geometry couples the fluid motion and the boundary motion through viscosity, and therefore the no-slip outer boundary condition is necessary to drive the precessing flow) and stress-free at the inner boundary to approximate a full sphere. The boundary condition for temperature deviation is homogeneous $\Theta = 0$. The magnetic boundary condition is insulating, namely, the magnetic field at the boundaries matches a potential field for the exterior regions of $r > r_o$ and $r < r_i$. The initial values of the flow, temperature deviation, and magnetic field are given as small values.

The equations are numerically solved in a spherical coordinate system (r, θ, ϕ) with a pseudo-spectral code (Tilgner 1999) which was used in Tilgner (2005) and Wei & Tilgner (2013). The toroidal-poloidal decomposition is used to take into account the solenoidal property of the fluid velocity and magnetic field. All of the functions are expanded with spherical harmonics on the spherical surface and with the Chebyshev polynomials in the radial direction. The semi-implicit scheme is employed for time stepping, using an Adams-Bashforth scheme for the nonlinear terms and a Crank-Nicolson scheme for the diffusive terms. Resolution as high as 128^3 is used and the resolutions are checked as in Tilgner (2005) and Wei & Tilgner (2013). To identify a successful dynamo, we integrate the MHD equations until the magnetic energy grows to a noticeable value and maintains for a long period without the tendency to decay.

3. RESULTS

As discussed in Tilgner (2005), both the laminar precessing flow at high Ekman number and the unstable precessing flow at low Ekman number can induce the dynamo action. In the Earth's core, the Ekman number is very low, of the order of 10^{-15} , and the precessing flow at such a low Ekman number is unstable. Therefore, we study the Ekman number $Ek = 3 \times 10^{-4}$ at which the precessing flow is already unstable (Tilgner 2005; Wei & Tilgner 2013). One may argue that this Ekman number is not low enough, e.g., 10^{-6} used in some large-scale simulations for the convection dynamo. It should be noted that the purpose of our study is to initiate the investigation of the combined effect of precession and convection on the dynamo, not to push the parameter toward the real Earth or to scan the parameter space for a systematic study. It is clear that at lower Ekman number, the precessing flow has more complex structure and exhibits higher azimuthal wavenumbers, which favors the dynamo action. At

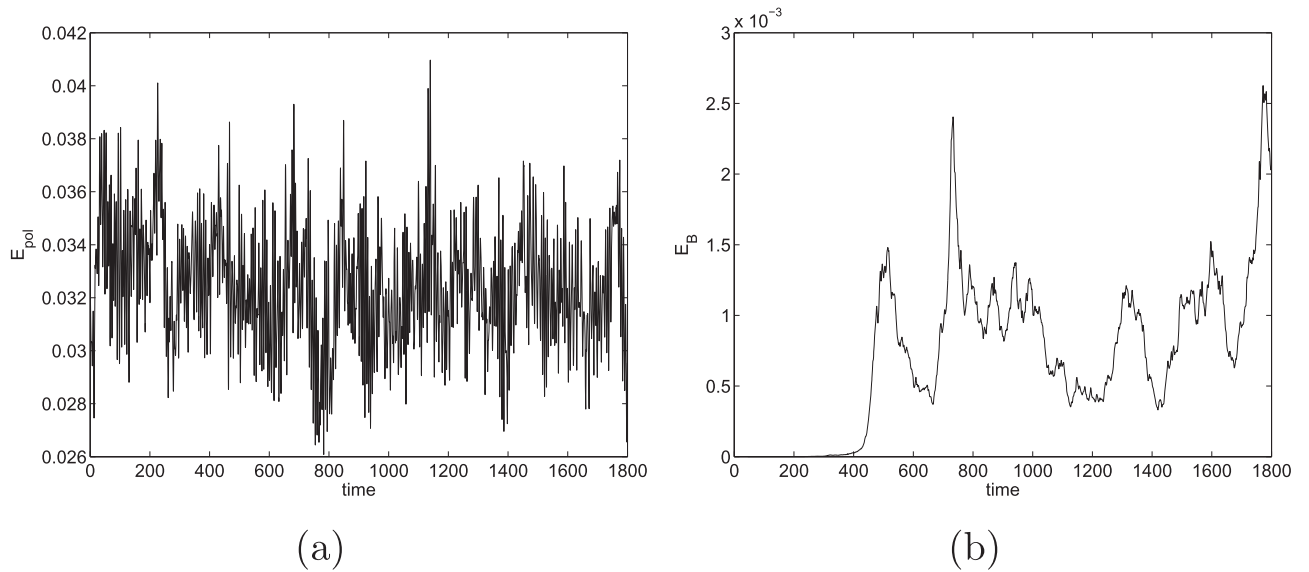


Figure 1. Precession dynamo at $Po = -0.3$. Here, we show the time evolution of the poloidal kinetic energy (a) and magnetic energy (b).

Table 1
The Successful and Failed Dynamos at Different Po and \widetilde{Ra}

(Po, \widetilde{Ra})	Ra	Nu	E_{pol}	Rm	m	E_B
$(-0.2, 0)$	0	n/a	3.11×10^{-2}	694	1	failed dynamo
$(-0.3, 0)$	0	n/a	3.23×10^{-2}	707	1	9.44×10^{-4}
$(0, 0.5)$	6.17×10^6	1.78	1.15×10^{-3}	133	3	failed dynamo
$(0, 0.6)$	7.41×10^6	1.83	1.33×10^{-3}	144	3	2.11×10^{-7}
$(-0.2, 0.5)$	6.17×10^6	2.20	2.96×10^{-2}	677	1	1.78×10^{-5}

Note. For the successful dynamos, the conventional Rayleigh number, the Nusselt number, the Poloidal kinetic energy, the dominant azimuthal mode of the flow, and the magnetic energy are shown. The values are taken for the time average in the statistically steady stage.

$Ek = 3 \times 10^{-4}$, the precessing flow is already unstable and the important physical ingredient that an unstable precessing flow favors the dynamo action is already involved. Therefore, we do not attempt to push the Ekman number to smaller values due to the limitation of our computational facility.

We calculate step-by-step the precession dynamo, the convection dynamo, and the precession-convection dynamo. The Prandtl number Pr is fixed to be 1. It is known that a higher magnetic Prandtl number Pm facilitates the onset of a dynamo (see Figure 1 in Christensen & Aubert 2006 or Figure 8 in Jones 2011), and it is fixed at 2, which is above the critical Pm . We then vary Po and \widetilde{Ra} to search for the dynamo. Because the Earth's precession is retrograde, Po is given to be negative.

First, we study the precession dynamo. Before calculating the precession dynamo, we calculate the hydrodynamic precessing flow. These numerical calculations give the fluid rotation vector to be consistent with Busse's solution derived from the Ekman-layer asymptotic calculation (Busse 1978). We do not repeat to show the hydrodynamic results in this paper, which have already been discussed in detail in Tilgner (2005) and Wei & Tilgner (2013) using the same numerical setup and code. Now, we vary Po to calculate the nonlinear dynamo equations at $Ek = 3 \times 10^{-4}$, $Pr = 1$, and $Pm = 2$ to search the critical $|Po|$ for the onset of the dynamo. We increase $|Po|$ by a step of 0.1. It is found that magnetic energy eventually decays at $Po = -0.2$, but grows and eventually saturates at $Po = -0.3$. Therefore, the critical $|Po|$ for the precession

dynamo is between 0.2 and 0.3. At such a low Ekman number, the precessional instabilities develop such that the symmetry of the laminar precessing flow about the center ($r=0$) breaks, and so the instabilities can be measured by the kinetic energy of the anti-symmetric component of the flow $\mathbf{u}_a = [\mathbf{u}(\mathbf{r}) + \mathbf{u}(-\mathbf{r})]/2$ (Tilgner 2005; Wei & Tilgner 2013). It should be noted that the precessional instabilities contain both anti-symmetric and symmetric components, but the laminar precessing flow contains only the symmetric component, and so the non-zero anti-symmetric component indicates the precessional instabilities and the energy of the anti-symmetric component measures the strength of the precessional instabilities. Figure 1 shows the time evolution of the precession dynamo at $Po = -0.3$, which is consistent with the result in Tilgner (2005). The ratio of the anti-symmetric kinetic energy to the total kinetic energy E_a/E_{kin} is not negligible and its time average is 5.34×10^{-3} , which indicates that the precessing flow is unstable. The poloidal flow is important for the α effect in dynamo action, i.e., twisting field lines. Figure 1(a) shows the time evolution of the poloidal kinetic energy. Its time average is listed in Table 1. As in Tilgner (2005), we define the magnetic Reynolds number Rm with the dimensionless mean poloidal flow $u_{\text{pol}} = \sqrt{2E_{\text{pol}}/V}$ (where E_{pol} is the poloidal energy of flow and V is the fluid volume) to be $Rm = u_{\text{pol}}Pm/Ek$. Rm is 707 at $|Po| = 0.3$ (Table 1) for a successful dynamo, but 694 at $|Po| = 0.2$ for a failed dynamo. The dominant azimuthal mode of the precessing flow is $m = 1$,

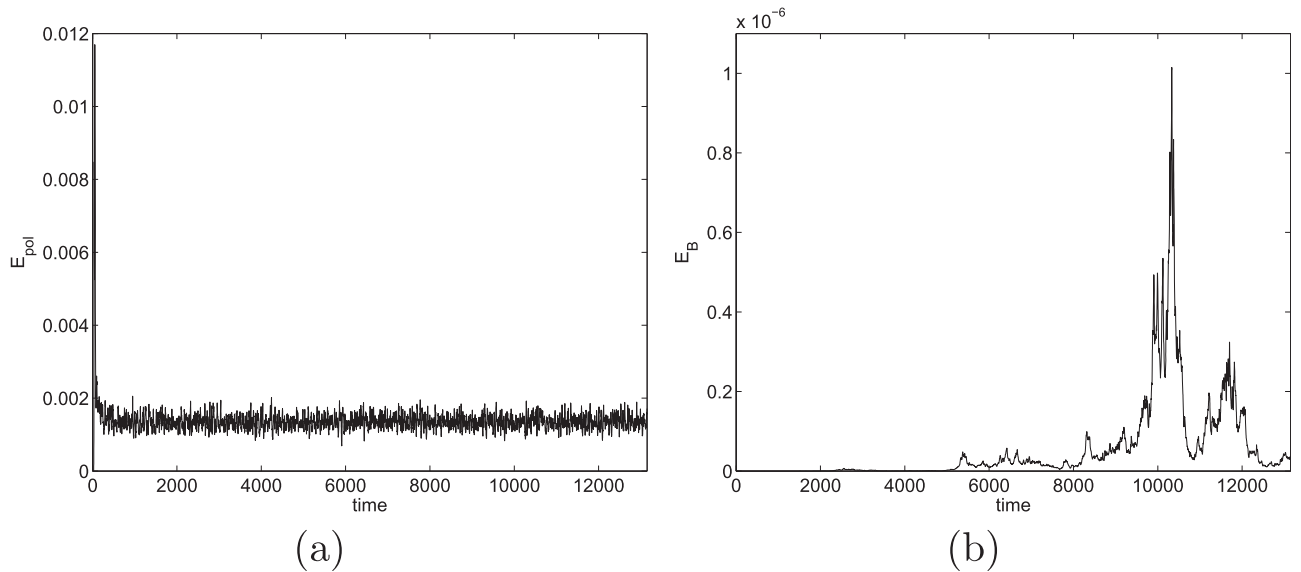


Figure 2. Convection dynamo at $\widetilde{Ra} = 0.6$. Here, we show the time evolution of the poloidal kinetic energy (a) and the magnetic energy (b).

i.e., the spin-over mode (Greenspan 1968; Tilgner 2007). Figure 1(b) shows the time evolution of the magnetic energy. A comparison of Figures 1(a) and (b) indicates that the flow fluctuates on a small scale, whereas the magnetic field varies on a large timescale. The time average of the magnetic energy E_B is also listed in Table 1.

Next, we study the convection dynamo. Similar to the precession dynamo, we vary \widetilde{Ra} to search for the onset of the convection dynamo. It is found that the critical \widetilde{Ra} is between 0.5 and 0.6, i.e., the magnetic energy decays at $\widetilde{Ra} = 0.5$ but grows and saturates at $\widetilde{Ra} = 0.6$. Figure 2 shows the time evolution of the convection dynamo at $\widetilde{Ra} = 0.6$. We should emphasize that although the difference of \widetilde{Ra} is only 0.1, the conventional Ra translated through Equation (6) is more than one million (see Table 1)! In a convective flow, the Nusselt number Nu is used to measure the ratio of the total heat flux to the thermal conduction. The time average of Nu at the outer boundary is 1.83 (Table 1), which indicates a strong convective motion (Nu at the inner boundary can be deduced from its value at the outer boundary through Equation (4.2) in Wei & Tilgner 2013). Figure 2(a) shows the time evolution of the poloidal kinetic energy. The poloidal kinetic energy of the convection dynamo is much lower than that of the precession dynamo, and thus $Rm = 144$ for the convection dynamo is lower than $Rm = 707$ for the precession dynamo (Table 1). As we discussed in the last paragraph, at $Rm = 694$, the precessing flow cannot maintain a dynamo, but the convective flow can at $Rm = 144$. In this sense, convection is more efficient for the onset of the dynamo than precession. We must point out that this conclusion is valid only at this Ekman number. At a smaller Ekman number, the precessing flow is more complex, which favors the onset of the dynamo, and this conclusion may not hold any longer (we leave the large-scale simulations at smaller Ekman numbers for other researchers who will be interested in the result of this work). The comparison between Figures 1(a) and 2(a) suggests that not only the mean poloidal kinetic energy but also the fluctuation amplitude of the precessing flow are much higher than those of the convective flow. This implies that the precessional instabilities are more

vigorous than the convective instabilities in the two successful dynamos. The dominant azimuthal mode in the convective flow is $m = 3$ (Table 1), indicating a shorter length scale than the dominant spin-over mode $m = 1$ in the precessing flow. Figure 2(b) shows the time evolution of the magnetic energy. Compared to Figure 1(b), the magnetic energy of the convection dynamo becomes noticeable at the time ≈ 5000 , which is much later than the time ≈ 400 of the precession dynamo. It is not surprising that the magnetic energy of the convection dynamo is also much lower than that of the precession dynamo (Table 1) because of the lower Rm of the former.

After studying the dynamos driven by precession alone and by convection alone, we study the combined effect of precession and convection. In the above two dynamos, the dynamo driven by precession alone cannot be maintained at $Po = -0.2$ and the dynamo driven by convection alone cannot be maintained at $\widetilde{Ra} = 0.5$. We test whether the precession-convection dynamo can be maintained at $Po = -0.2$ and $\widetilde{Ra} = 0.5$. This dynamo works! It indicates that the combined effect of precession and convection can indeed facilitate the onset of the dynamo. As we discussed, the conventional Ra differs by more than one million, which indicates that precession greatly helps the onset of the convection dynamo. Moreover, it is interesting that the $Rm = 677$ of the precession-convection dynamo is lower than the $Rm = 694$ of the failed precession dynamo, as shown in Table 1. This suggests that the combination of precession and convection has some non-trivial effect and triggers the dynamo action at a lower Rm of the pure precession dynamo. This non-trivial effect probably arises from the resonance of precessional instability and convective instability. Figure 3 shows the time evolution of this precession-convection dynamo and its time-averaged values are listed in Table 1. Although the $\widetilde{Ra} = 0.5$ of the precession-convection dynamo is lower than the $\widetilde{Ra} = 0.6$ of the convection dynamo, the Nu of the former is higher (Table 1). This is because the poloidal flow driven by precession contributes more to heat transfer than convection, i.e., $E_{\text{pol}} = 3.11 \times 10^{-2}$ of the precessing flow at $Po = -0.2$ is already much higher than $E_{\text{pol}} = 1.33 \times 10^{-3}$ of the

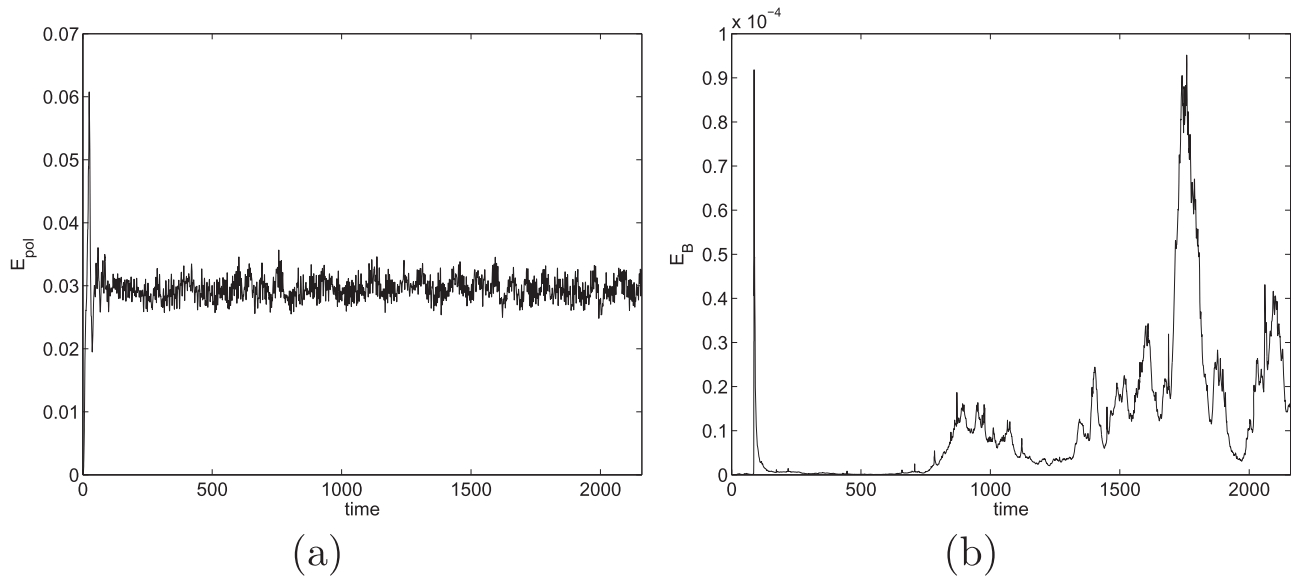


Figure 3. Precession-convective dynamo at $Po = -0.2$ and $\tilde{Ra} = 0.5$. Here, we show the time evolution of the poloidal kinetic energy (a) and the magnetic energy (b).

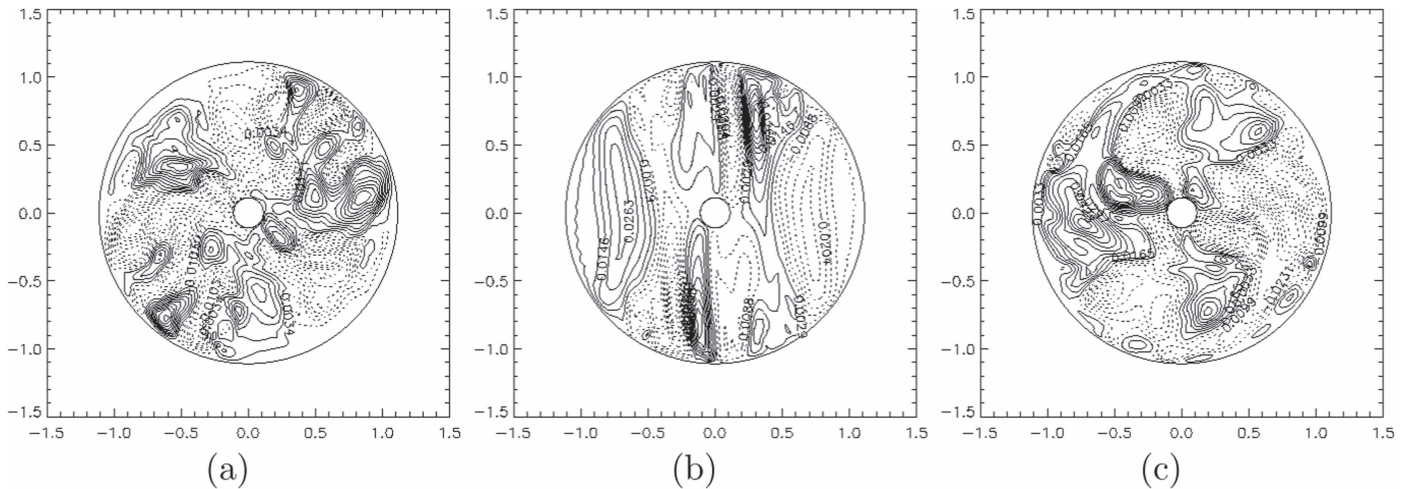


Figure 4. Contours of the radial velocity in the meridional plane at $\phi = 180^\circ$. (a) The precession dynamo at $Po = -0.3$. (b) The convection dynamo at $\tilde{Ra} = 0.6$. (c) The precession-convective dynamo at $(Po = -0.2, \tilde{Ra} = 0.5)$. Solid lines denote positive and dotted lines negative. These are all snapshots when the dynamos saturate.

convective flow at $\tilde{Ra} = 0.6$. The dominant azimuthal mode is $m = 1$ (Table 1), which indicates that the precession-convective flow is more precessing than convective. E_{pol} and Rm of the precession-convective dynamo are a little lower than those of the precession dynamo but much higher than those of the convection dynamo (Table 1), which again suggests that the precession-convective flow is more precessing. The magnetic energy becomes noticeable at time ≈ 700 (Figure 3(b)), which is a little later than the time ≈ 400 of the precession dynamo but much earlier than the time ≈ 5000 of the convection dynamo.

To end this section, we discuss the flow patterns in the different dynamos. Figure 4 shows the contours of the radial velocity in the meridional plane in the precession, convection, and precession-convective dynamos. The flow of the convection dynamo exhibits the columnar structure at such low Ek . However, the flow of the precession dynamo seems chaotic because, as discussed, the precessional instabilities are more vigorous than the convective instabilities. The flow of the

precession-convective dynamo is similar to that of the precession dynamo and has a more complex structure than the flow of the convection dynamo. This also explains why the combined effect favors the dynamo action. It is because the precession-convective flow tends to be chaotic and have the complex structure which favors the dynamo action.

4. SUMMARY

Through our numerical calculations, we know that the combined effect of precession and convection favors the dynamo action. Although precession alone or convection alone is not strong to support the dynamo action, the combined precession-convective dynamo works. The reason for this is that the combined effect tends to make the flow more unstable and a more complex flow structure emerges which favors the dynamo action. Thus, we may have a tentative point. After a long history, the heat flux in the Earth's fluid core becomes weaker and weaker and at some time the convection is not

powerful to support the geodynamo (e.g., Olson 2013), but the geodynamo can still be maintained because the precession provides the energy. This could have already occurred in Earth's early history when the fluid core was too small to support the geodynamo. This could be occurring in the Earth's core. This could occur in the future because the heat flux in the Earth's fluid core diminishes and will not support the geodynamo. In comparison, the Martian dynamo terminated because the precession of Mars is not as strong as that of the Earth. When the convection in the Martian fluid core stopped, the Martian dynamo could not be maintained by the weak Martian precession. It should be clarified that this is our tentative conjecture and requires additional observational evidence to support or refute.

In addition to the Earth's magnetic field, the result of this work can be extended to the magnetic fields of small bodies. Wei et al. (2014) studied the dynamo action in small bodies driven by collisions. Precession can be considered as continuous collisions when the collision frequency is close to infinitesimal. In the presence of both collision and convection, it is plausible that the dynamo due to collisions tends to be driven more easily than by collision or convection alone.

There is further work that we leave for interested researchers. The Ekman number in this work is not very small, although it is sufficiently small for the onset of precessional instabilities. Our work simply initiates the study of the combined effect of precession and convection. As we know, the precessing flow structure at lower Ekman numbers will be complex and instabilities will prefer higher azimuthal modes. Therefore, the low Ekman regime must be investigated. Another area of further study is the geometry. In this work, we study a spherical dynamo. The Earth's core is not spherical but spheroidal. The pressure torque in the spheroidal geometry can enhance the coupling between fluid and boundary motions (Tilgner 2007), and, moreover, elliptical instability in spheroidal geometry, an instability of a two-dimensional flow with elliptical streamlines leading to a three-dimensional flow (Kerswell 2002; Tilgner 2007; Zhang et al. 2014), can occur. Both the pressure torque and the elliptical instability can facilitate the dynamo

action. Therefore, the spheroidal geometry also must be investigated.

This work was initiated in Princeton and completed in Shanghai. Prof. Andreas Tilgner provided me his code. Prof. Andreas Tilgner and Prof. Keke Zhang provided valuable suggestions about this work. This work was supported by the National Science Foundations Center for Magnetic Self-Organization under grant PHY-0821899 and the startup grant WF220441903 of Shanghai Jiao Tong University.

REFERENCES

- Bullard, E., & Gellman, H. 1954, *RSPTA*, 247, 213
 Busse, F. H. 1968, *JFM*, 33, 739
 Busse, F. H. 1978, *AnRFM*, 10, 435
 Cébron, D., Meunier, P., & Le Bars, M. 2010, *GeoJ*, 182, 1311
 Christensen, U. R., & Aubert, J. 2006, *GeoJI*, 166, 97
 Ernst-Hullermann, J., Harder, H., & Hansen, U. 2013, *GeoJI*, 195, 1395
 Goto, S., Matsunaga, A., Fujiwara, M., et al. 2014, *PhFI*, 26, 055107
 Greenspan, H. P. 1968, *Theory of Rotating Fluids* (Cambridge, UK: Cambridge Univ. Press)
 Hollerbach, R. 1996, *PEPI*, 98, 163
 Hollerbach, R., Nore, C., Marti, P., et al. 2013, *PhRvE*, 87, 053020
 Jones, C. A. 2011, *AnRFM*, 43, 583
 Kerswell, R. 1993, *GApFD*, 72, 107
 Kerswell, R. 2002, *AnRFM*, 34, 83
 Lavorel, G., & Le Bars, M. 2010, *PhFI*, 22, 114101
 Lin, Y., Noir, J., & Jackson, A. 2014, *PhFI*, 26, 046604
 Malkus, W. V. R. 1968, *Sci*, 160, 259
 Noir, J., Cardin, P., Jault, D., & Masson, J. P. 2003, *GeoJI*, 154, 407
 Olson, P. 2013, *Sci*, 342, 431
 Poincaré, H. 1910, *Bull. Astron.*, 27, 321
 Roberts, P. H., & Glatzmaier, G. A. 2000, *RvMP*, 72, 1081
 Tilgner, A. 1999, *IJNMF*, 30, 713
 Tilgner, A. 2005, *PhFI*, 17, 034104
 Tilgner, A. 2007, in *Treatise on Geophysics*, ed. G. Schubert (Amsterdam: Elsevier)
 Wei, X., Arlt, R., & Tilgner, A. 2014, *PEPI*, 231, 30
 Wei, X., & Tilgner, A. 2013, *JFM*, 718, R2
 Wu, C.-C., & Roberts, P. 2009, *GApFD*, 103, 467
 Yamazaki, T., & Oda, H. 2002, *Sci*, 295, 2435
 Zhang, K., Chan, K. H., & Liao, X. 2014, *JFM*, 743, 358
 Zhang, K., & Schubert, G. 2000, *AnRFM*, 32, 409